AAPS PharmSciTech, Vol. 15, No. 1, February 2014 (© 2013)
DOI: 10.1208/s12249-013-0034-2

Research Article

Enhanced Topical Delivery of Finasteride Using Glyceryl Monooleate-Based Liquid Crystalline Nanoparticles Stabilized by Cremophor Surfactants

Thiagarajan Madheswaran,[1] Rengarajan Baskaran,[2] Chul Soon Yong,[1] and Bong Kyu Yoo[2,3]

Received 30 May 2013; accepted 10 September 2013; published online 25 September 2013

Abstract. The aim of this study was to investigate the capability of two surfactants, Cremophor RH 40 (RH) and Cremophor EL (EL), to prepare liquid crystalline nanoparticles (LCN) and to study its influence on the topical delivery of finasteride (FNS). FNS-loaded LCN was formulated with the two surfactants and characterized for size distribution, morphology, entrapment efficiency, *in vitro* drug release, and skin permeation/retention. Influence of FNS-loaded LCN on the conformational changes on porcine skin was also studied using attenuated total reflectance Fourier-transform infrared spectroscopy. Transmission electron microscopical image confirmed the formation of LCN. The average particle size of formulations was in the range of 165.1–208.6 and 153.7–243.0 nm, respectively. The formulations prepared with higher surfactant concentrations showed faster release and significantly increased skin permeation. Specifically, LCN prepared with RH 2.5% presented higher permeation flux (0.100± 0.005 $\mu gcm^{-2}h^{-1}$) compared with lower concentration (0.029±0.007 $\mu gcm^{-2}h^{-1}$). Typical spectral bands of lipid matrix of porcine skin were shifted to higher wavenumber, indicating increased degree of disorder of the lipid acyl chains which might cause fluidity increase of stratum corneum. Taken together, Cremophor surfactants exhibited a promising potential to stabilize the LCN and significantly augmented the skin permeation of FNS.

KEY WORDS: Cremophor; finasteride; liquid crystalline nanoparticles; skin permeation–retention.

INTRODUCTION

Finasteride (FNS) is a potent antiandrogen used in the treatment of male pattern baldness or androgenetic alopecia (AGA) (1,2). In AGA, increased level of dihydrotestosterone (DHT) has been observed in scalp skin which causes miniaturization of hair follicles and progressive loss of hair (3,4). FNS acts by specifically inhibiting type II 5-α reductase responsible for the conversion of testosterone to DHT (5). Although oral administration of FNS effectively increased the hair counts, its systemic exposure causes various sexual side effects, particularly erectile dysfunction and ejaculatory disorder (6,7). In this regard, it was hypothesized that topical delivery would overcome the side effects associated with oral administration. Hence, there is a growing interest in the development of suitable topical carrier systems to deliver FNS to target sites (8,9). However, development of successful topical carrier has been limited by the barrier function exerted by the stratum corneum (SC).

Various approaches have been developed to overcome the skin barrier function and to enhance the permeation of drug across skin layers (10). One of the novel approaches is the utilization of nanoparticulate system as a vehicle to promote the skin delivery of bioactive molecules (11,12). Recently, there has been growing interest in monoolein (MO)-based liquid crystalline nanoparticle (LCN) as a topical carrier system (13–15). LCN is composed of highly twisted lipid bilayer and two non-intersecting water channels. This unique nanostructure affords high solubilization capacity of the bioactive molecules and exhibits controlled release from the LCN (16,17). In addition, LCN can be easily prepared and offers many advantages such as improved stability, biocompatibility, and biodegradability (18). LCNs are prepared by nano-sized fragmentation of bulk liquid crystalline phase formed from MO-water system using homogenization or sonication (19). However, LCN system needs surfactant to form a kinetically stable dispersion. The stabilization of these nanoparticles used to be accomplished by incorporating block copolymers, most commonly poloxamer 407 (P407) (20).

In our efforts to enhance the topical delivery of FNS, we have already demonstrated that LCN enhances permeation and retention of the drug in skin (21). Given that this nanocarrier is a promising topical delivery vehicle, development of alternate stabilizer other than P407 may have profound impact on FNS-containing topical delivery system. We have hypothesized that surfactant plays major role in skin permeation of FNS when the drug is applied as topical formulation of MO-based LCN. Polyoxyethylated nonionic surfactants have been widely utilized in the preparation of microemulsion, self-emulsifying system,

[1] College of Pharmacy, Yeungnam University, 214-1 Dae-dong, Gyeongsan 712-749, South Korea.
[2] College of Pharmacy, Gachon University, 191 Hambakmoero, Incheon 406-799, South Korea.
[3] To whom correspondence should be addressed. (e-mail: byoo@gachon.ac.kr)

and solid lipid nanoparticles (22–24). Moreover, these surfactants have shown to enhance skin permeation of drugs such as terbinafine and interferon alpha (24,25). Among the various polyoxyethylated nonionic surfactants, we have chosen Cremophor RH 40 (RH) and Cremophor EL (EL) because their HLB values are in the range of 12–16 which are appropriate for the preparation of MO-based LCN dispersion. In this study, we investigated the influence of two polyoxyethylated nonionic surfactants, RH and EL, on the skin permeation and retention of FNS using porcine skin.

MATERIALS

MO was received as a gift from Danisco Japan (Tokyo, Japan). FNS was kindly donated from Dong-A Pharmaceutical Co, South Korea. Poloxamer 407, RH, and EL were purchased from BASF (Ludwigshafen, Germany). Dialysis membrane was purchased from Spectrum Laboratories Inc (California, USA). All other chemicals were of analytical grade and used without further purification.

METHODS

Preparation of FNS-Loaded LCN

LCN was prepared with slight modification of previously reported method (21), and composition of formulation is given in Table I. Briefly, appropriate amounts of MO and surfactant were melted at 45°C in a glass vial, and FNS was added with vortexing (solubility of FNS, >100 mg/ml of MO at 45°C). To this molted mixture, distilled water heated at the same temperature was added and vortexed. The coarse dispersion formed was subjected to sonication for 30 min using bath type sonicator (Cole-Parmer Ultrasonic 8893, USA) at 42,000 Hz.

Characterization of FNS-Loaded LCN

Dynamic Light Scattering and Zeta Potential

Hydrodynamic size, polydispersity index, and zeta potential were determined by using Zetasizer Nano ZS (Malvern Instruments, UK). The instrument was equipped with dynamic light scattering particle size analyzer at a wavelength of 635 nm and a fixed scattering angle of 90°. All samples were analyzed in triplicate, and the values of z-average diameters were used. Before analysis, the dispersion was suitably diluted with distilled water (18.2 MΩ cm^{-1}) and measured at 25°C.

Transmission Electron Microscopy (TEM)

Morphology of LCN was photographed by using a transmission electron microscope (Hitachi 7600, Japan) at an accelerating voltage of 100 kV. Briefly, one drop of nanoparticle dispersion was deposited on carbon-coated copper grid to form a thin liquid film. The grid was negatively stained immediately by adding a drop of 1% *w/w* phosphotungstic acid, followed by air-drying at room temperature for 5 min.

Entrapment Efficiency (EE)

EE was determined by ultrafiltration method using specialized ultrafilter tube (Amicon Ultra-4, MWCO 10,000 g/mole, USA) as described elsewhere (21). Briefly, 1 ml of LCN dispersion was transferred to the upper chamber of ultrafiltration tube and centrifuged at 2,500×*g* for 15 min. The filtrate containing free FNS was analyzed by HPLC, and EE was calculated by following equation—$EE\ (\%) = 100\times(D_{\text{tota l}} - D_{\text{free}})/D_{\text{total}}$, where D_{total} is amount of total FNS and D_{free} is amount of free FNS in the LCN dispersion, respectively. The HPLC system (Shimadzu) consists of LC 20 AD pump, SPD 20A UV–VIS detector at 210 nm attached with SIL 20A prominence autosampler. The column used was Inertsil ODS-3 (4.6×150 mm, GL Science, Japan), and mobile phase consisted of mixture of acetonitrile and water (60:40 *v/v*, pH adjusted to 2.8 with orthophosphoric acid). Ibuprofen was used as internal standard, and injection volume was 20 μl with flow rate of 1 ml/min.

Viscosity Measurements

Viscosity of nanoparticle dispersions were determined using rotational viscometer (Merlin VR, USA) equipped with a 30 mm parallel plate system. LCN dispersions were laid on the plate to determine shear rate and shear stress, and the temperature was automatically controlled at 20±0.1°C. A software program (Micra, USA) was used to record flow curves with increasing shear rates from 1 to 100 s^{-1}, and viscosity was calculated.

In Vitro Drug Release Study

The *in vitro* drug release was evaluated by Franz diffusion cell with effective diffusion area of 2.1 cm^2 using artificial membrane made of regenerated cellulose with MWCO 10,000 g/mole (Spectra/Por®, Spectrum Laboratories). The membrane was mounted between donor and receptor compartments, and FNS dispersion (0.5 ml) was applied evenly on the donor compartment. The receptor compartment was filled with 10 ml of 20% *v/v* ethanol in phosphate buffer saline (pH 7.4) and maintained at 32± 0.5°C with magnetic stirring. Samples (500 μl) were withdrawn at fixed time intervals (1, 2, 3, 6, 12, and 24 h) from the receptor compartment and replaced with fresh buffer solution. The samples were then analyzed for FNS content using HPLC.

In Vitro Skin Permeation and Retention Studies

Franz diffusion cell with diffusion area of 2.1 cm^2 was used for skin permeation and retention study. The experiments were performed using porcine abdominal skin obtained from a local abattoir house. The skin was dermatomed (700–800 μm thick) and stored frozen at −20°C until used. Before 2 h of the experiments, skin samples were pre-equilibrated in phosphate buffer saline (pH 7.4) at room temperature and then mounted between donor and receptor compartments with stratum corneum facing the donor compartment. The receptor compartment was filled with 10 ml of 20% *v/v* ethanol in the phosphate buffer saline and maintained at 32±0.5°C using

Table I. Compositions of MO-Based LCN Containing FNS and Its Characterization Parameters

Formulation code	MO (% *w/w*)	P407 (%*w/w*)	FNS (%*w/w*)	RH (%*w/w*)	EL (%*w/w*)	Distilled water (%*w/w*)	Particle size (nm)	PDI	Zeta potential	Entrapment efficiency (%)	Viscosity (mPa s)
RH 0.5	4	–	0.1	0.5	–	95.4	165.1±3.8	0.22 ±0.01	−24.3±0.5	99.4±0.1	7.8±0.7
RH 1.0	4	–	0.1	1.0	–	94.9	162.3±1.0	0.20±0.02	−24.6±0.6	99.3±0.1	8.2±0.4
RH 1.5	4	–	0.1	1.5	–	94.4	159.2±1.7	0.15±0.02	−23.3±0.9	99.4±0.1	8.7±0.2
RH 2.0	4	–	0.1	2.0	–	93.9	174.2±2.1	0.10±0.01	−23.1±0.7	99.2±0.2	8.8±0.2
RH 2.5	4	–	0.1	2.5	–	93.4	208.6±1.9	0.07±0.02	−22.1±0.8	99.3±0.1	8.8±0.2
EL 1.5	4	–	0.1	–	1.5	94.4	153.7±2.6	0.23±0.01	−22.8±0.9	98.9±0.1	7.1±2.8
EL 2.0	4	–	0.1	–	2.0	93.9	163.0±1.6	0.19±0.01	−23.9±0.6	98.9±0.2	8.5±0.5
EL 2.5	4	–	0.1	–	2.5	93.4	163.4±1.6	0.18±0.01	−22.2±0.9	98.9±0.2	8.8±0.2
EL 3.0	4	–	0.1	–	3.0	92.9	185.2±2.2	0.18±0.01	−22.6±0.2	99.0±0.1	8.8±0.7
EL 4.0	4	–	0.1	–	4.0	91.9	243.0±9.2	0.11±0.02	−22.0±0.3	99.2±0.1	9.3±0.3
P407	4	1.0	0.1	–	–	94.9	167.0±1.3	0.20±0.02	−21.5±0.4	99.6±0.1	8.8±0.4

Each value represents the mean±SD (n=3)
MO monoolein, *P407* poloxamer 407, *FNS* finasteride, *RH* cremophor RH 40, *EL* cremophor EL

magnetic stirrer. FNS-loaded LCN dispersion and control (FNS dissolved in 20% *v/v* ethanol) containing 500 μg FNS were applied onto the skin and sealed with Parafilm® to prevent water evaporation. Samples from receptor compartment were collected at predetermined time interval (1, 2, 3, 6, 12, and 24 h) and replaced with the same volume of fresh medium.

The cumulative amount of FNS permeated through porcine skin per unit surface area was plotted as a function of time. The steady-state flux (J_{ss}, micrograms per centimeter per

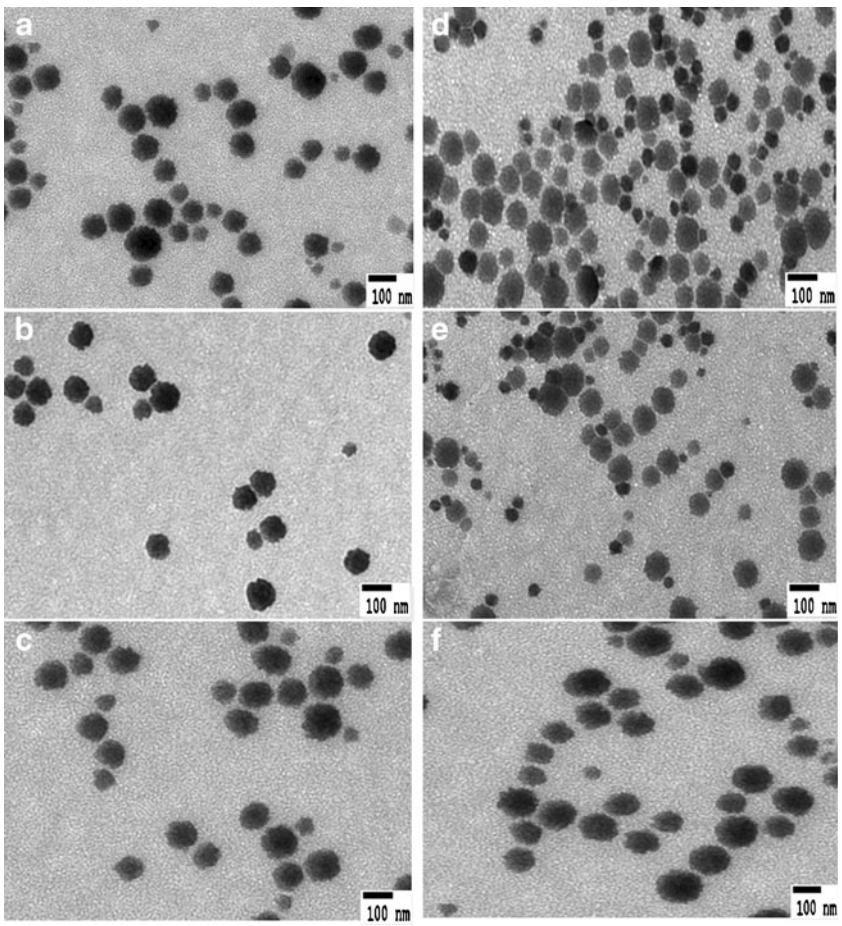

Fig. 1. TEM image of blank LCN **a-c** and FNS-loaded LCN **d-f**. **a**, **d** Prepared with RH. **b**, **e** prepared with EL. **c**, **f** Prepared with P407

hour) was calculated from the slope of linear regression interpolation, and lag time (T_L, hours) was equal to the intercept of *X*-axis. The slope and intercept were derived using GraphPad Prism® v.4.00 software. The permeability coefficients was calculated as $K_p = Jss/[(DC_i + DC_f)/2]$, where DC_i and DC_f are the initial and final concentration of the donor compartment, respectively.

At the end of the permeation study, amount of FNS retained in the skin was determined as described below. Skins were washed with distilled water, minced with surgical scalpel, and added to glass vial containing 4 ml of acetonitrile water mixture (60:40, *v/v*) followed by homogenization (Ultra-Turrax T25 Basic, Germany) under ice bath for 5 min and sonication for 20 min. The resulting mixture was then filtered using 0.45 μm membrane filter and assayed for FNS using HPLC.

Attenuated Total Reflectance Fourier-Transform Infrared Spectroscopy (ATR-FTIR)

Fourier-transform infrared (FTIR) spectroscopic studies were performed using FTIR spectrophotometer equipped with attenuated total reflectance (ATR) (Tensor 27, Bruker Optics, Germany) containing photovoltaic mercury cadmium telluride (MCT) detector at 25°C. Samples for FTIR analysis were obtained by treating the skin for 6 h with same conditions as permeation and retention study. After treatment, spectra were obtained in the frequency range of 4,000–400 cm^{-1} by placing stratum corneum layer exposed to surface of ZnSe crystal, and the spectral data were analyzed using software OPUS 6.5.

Statistical Analysis

All the data obtained were analyzed by Student's *t*test using Microsoft Office Excel 2010. Data are presented as mean±standard deviation. A value of $p<0.05$ was considered statistically significant.

RESULTS

FNS-loaded LCN was prepared by ultrasonication method using bath type sonicator. Optimal surfactant concentration was judged by ability to form milky dispersion without apparent visible aggregates or phase separation during a week after preparation. The optimal surfactant concentration was in the range of 0.5–2.5% *w/w* and 1.5–4.0% *w/w* for RH and EL, respectively. Although, milky dispersion was formed out of

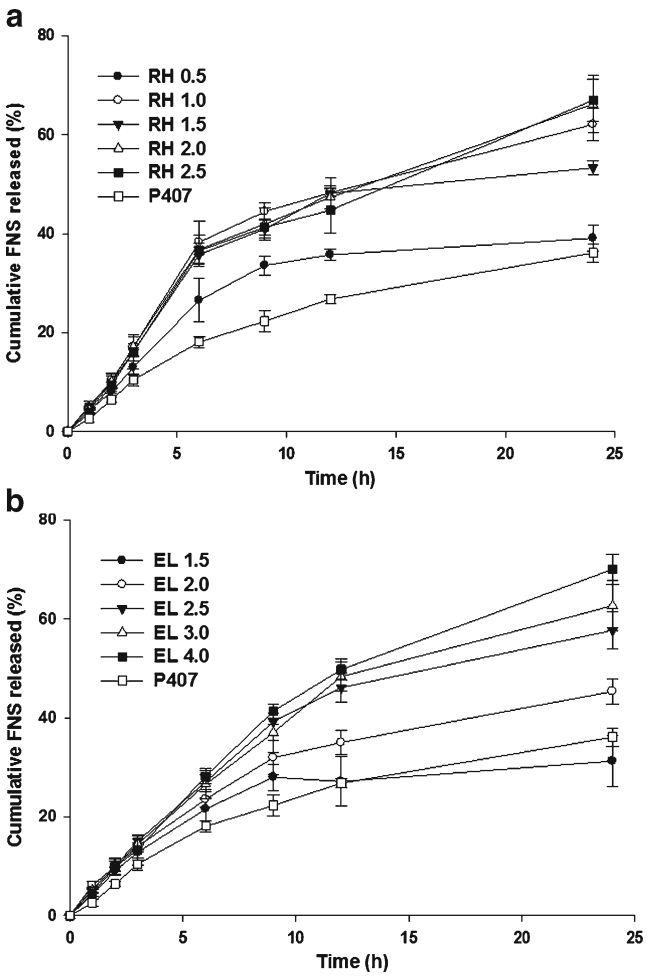

Fig. 2. Cumulative release profile of FNS from LCN. Each value represents mean±SD ($n=3$). **a** Prepared with RH. **b** Prepared with EL

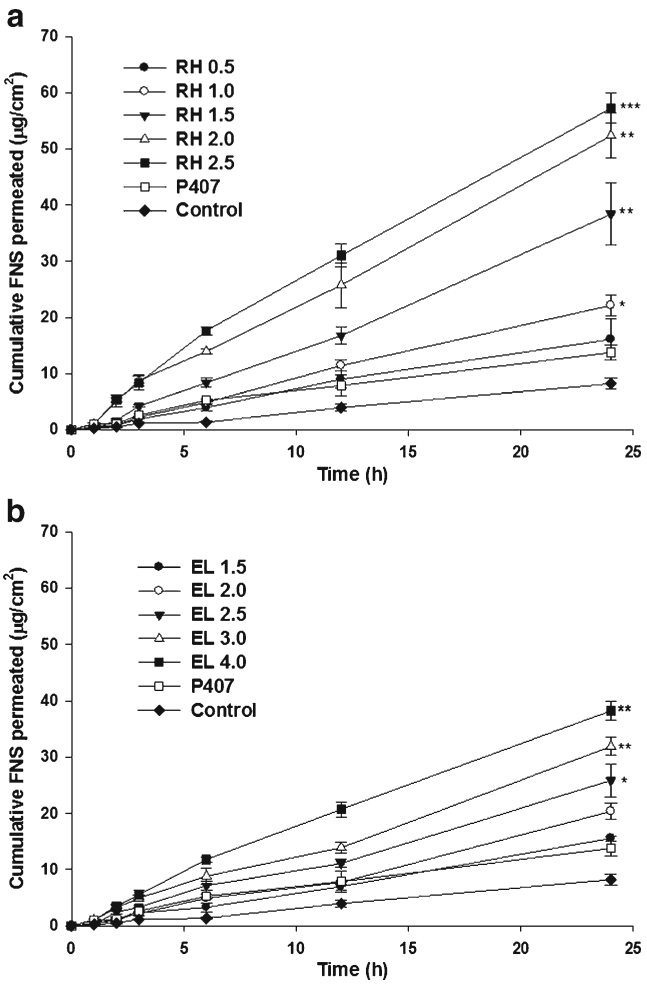

Fig. 3. Permeation profile of FNS-loaded LCN through porcine skin. Each value represents mean±SD ($n=3$). **a** LCN prepared with RH. **b** LCN prepared with EL. *$p<0.05$, **$p<0.01$, ***$p<0.001$ compared with control

the optimal range, it showed visible aggregates and resulted in phase separation within a day.

The average particle size of FNS-loaded LCN prepared with various concentrations of RH and EL were in the range of 165.1–208.6 and 153.7–243.0 nm, respectively (Table I). There was no significant difference in the particle size among the formulations prepared with same concentration of RH, EL, and P407. However, the size was increased in proportion to the concentration of RH and EL. The PDI values were lower than 0.3 for all the formulations regardless of the surfactant concentration. This result indicates the suitability of the preparation method and monodispersed particle size distribution. Zeta potential was slightly more negative in the LCN prepared with RH and EL compared with the LCN prepared with P407, but there was no significant difference (Table I). Figure 1a, b, c shows the transmission electron microscopy (TEM) images of blank LCN, and Fig. 1d, e, f shows FNS-loaded LCN. Both blank and FNS-loaded LCN displayed the formation of discrete and monodispersed nanoparticles. The images obtained from RH and EL were similar to that prepared with P407. Furthermore, drug loading did not influence the size of the nanoparticles and showed no apparent signs of aggregation. The particle size of blank LCN was in the range of 172.5–210.7 nm which was similar to the size of FNS-loaded LCN. The EE of FNS was found be above 98% for all formulations irrespective of surfactant concentrations (Table I).

Figure 2 shows release rate of FNS from LCN formulations prepared with varying concentration of surfactants. Interestingly, LCN prepared with RH depicted biphasic release profile showing faster release in the first 6 h and slower release afterward while the LCN prepared with EL or P407 did not. In terms of cumulative percent released in 24 h, RH resulted in greater release compared with EL—53.28% and 31.24% for RH 1.5% and EL 1.5%, respectively. Cumulative percentage of FNS released from LCN prepared with RH 2.5% was almost two times of those prepared with RH 0.5% and P407 1% at 24 h. A similar finding was observed with LCN prepared with EL.

The skin permeation measurements were carried out on Franz diffusion cell using porcine skin. Figure 3 shows the skin permeation profile of FNS from LCN formulations prepared with various concentrations of RH and EL. In accordance with the *in vitro* release study, higher surfactant concentration resulted in faster permeation rate. In particular, RH concentration of 1.0% or above resulted in statistically significant

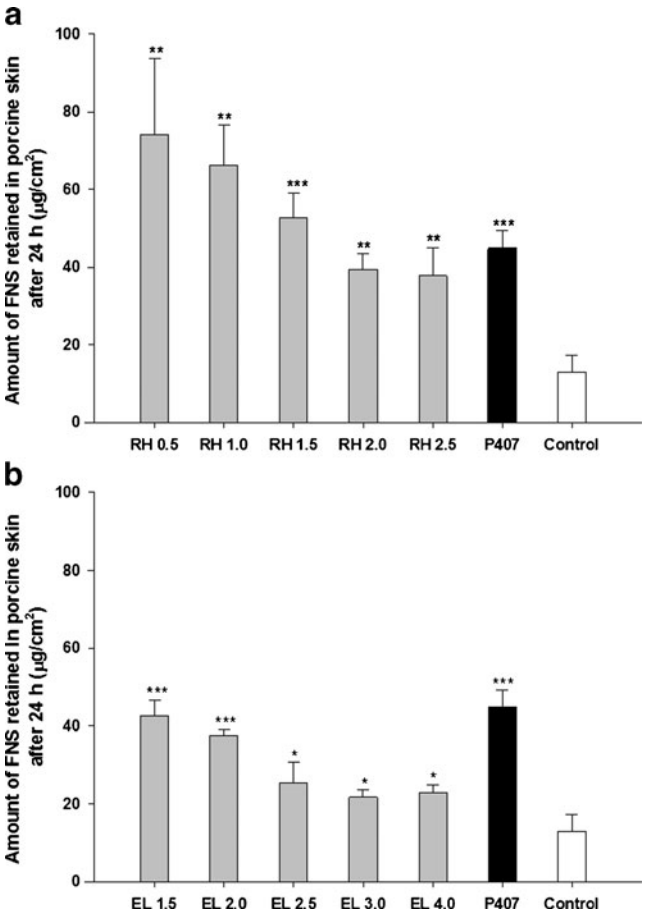

Fig. 4. Amount of FNS retained in porcine skin after 24 h of permeation study. Each value represents mean±SD (n=3). **a** LCN prepared with RH. **b** LCN prepared with EL. *p<0.05, **p<0.01, ***p<0.001 compared with control

Table II. Results of Skin Permeation and Retention Studies Using Porcine Skin

Formulation code	Permeation parameters				Percentage of FNS at the end of permeation study		
	J_{ss} (μg cm^{-2} h^{-1})	K_p (*10^{-4} cm h^{-1})	T_L (h)	ER	Receptor (%)	Donor (%)	Skin retention (%)
RH 0.5	0.029±0.007*	0.69±0.15*	1.46±0.39	1.99	3.2±0.7	67.6±8.3	23.7±6.3
RH 1.0	0.040±0.004$^{***,\#\#}$	0.96±0.08$^{***,\#\#}$	0.80±0.23	2.78	4.4±0.4	68.5±4.8	21.1±3.4
RH 1.5	0.068±0.009$^{***,\#\#}$	1.59±0.19$^{***,\#\#\#}$	0.89±0.31	4.71	7.7±1.1	72.1±2.4	16.9±2.0
RH 2.0	0.090±0.008$^{***,\#\#\#}$	2.17±0.28$^{***,\#\#\#}$	−0.27±0.02	6.19	10.5±0.8	66.0±7.5	12.7±1.2
RH 2.5	0.100±0.005$^{***,\#\#\#}$	2.44±0.13$^{***,\#\#\#}$	−0.40±0.08	6.88	11.4±0.5	63.5±5.2	11.1±1.5
EL 1.5	0.027±0.001***	0.62±0.03$^{***,\#}$	0.40±0.70	1.86	3.1±0.1	73.9±8.4	13.7±1.3
EL 2.0	0.035±0.003$^{***,\#\#}$	0.81±0.07$^{***,\#\#}$	0.74±0.25	2.43	4.1±0.3	75.0±4.8	12.1±0.4
EL 2.5	0.044±0.005$^{***,\#\#}$	0.99±0.10$^{***,\#\#}$	0.07±0.46	3.04	5.2±0.6	78.7±2.3	8.1±1.7
EL 3.0	0.049±0.007$^{\#,\#\#}$	1.15±0.21$^{\#,\#\#}$	−0.09±0.47	3.39	6.4±0.3	72.6±7.9	6.9±0.6
EL 4.0	0.067±0.003$^{***,\#\#\#}$	1.58±0.09$^{***,\#\#\#}$	−0.37±0.08	4.60	7.6±0.4	69.0±5.2	7.3±0.6
P407	0.023±0.002***	0.53±0.03$^{\#}$	−1.50±0.62	1.59	2.7±0.3	72.6±7.9	14.4±1.4
Control	0.014±0.002	0.33±0.03	0.62±0.47	–	1.6±0.2	78.2±4.1	4.1±1.4

Each value represents the mean±SD (n=3)
J_{ss} flux, K_p permeation coefficient, T_L lag time, *ER* enhancement ratio of flux compared with control (FNS dissolved in 20% *v/v* ethanol in PBS)
$^{*}p$<0.05, $^{**}p$<0.01, and $^{***}p$<0.001 compared with control; $^{\#}p$<0.05, $^{\#\#}p$<0.01, and $^{\#\#\#}p$<0.001 compared with P407

increase of permeation in proportional to the concentration. In terms of cumulative FNS permeated in 24 h, RH resulted in greater than twofold increase compared with EL—38.42 and 15.54 μgcm^{-2} for RH 1.5% and EL 1.5%, respectively. The flux (*J*), permeability coefficient (*Kp*), lag time (T_L), and enhancement ratio of the flux for each formulation were tabulated in Table II. Notably, the enhancement ratio showed 6.88-fold and 4.60-fold increase compared with control for RH 2.5% and EL 4.0%, respectively. Within the concentration range tested, RH showed better efficacy than EL and P407 in terms of enhancement ratio of the flux.

Figure 4 shows the effect of RH and EL concentration on the skin retention of FNS. In contrast to the results of the permeation study, retention of the drug was enhanced in the lower concentration of RH and EL. Specifically, amount of FNS retained in the porcine skin for RH 0.5% was 1.96-fold increase compared with RH 2.5%, and it was 1.86-fold for EL 1.5% compared with EL 4.0%.

Figure 5 depicts the spectra of porcine skin after treatment with distilled water and different LCN formulations prepared with lowest and highest concentration of the two surfactants. The spectrum depicts peaks in the regions, CH_2 asymmetric stretching (~2,918 cm^{-1}), CH_2 symmetric stretching (~2,850 cm^{-1}), C=O stretching (~1,736 cm^{-1}) and CH_2 scissoring (~1,457 cm^{-1}). Wave numbers characteristic of porcine skin were tabulated in Table III. For all the LCN formulations, the spectral bands shifted to higher wave number compared with untreated skin samples.

Table III. ATR-FTIR Characteristic Bands of Porcine Skin After Treatment with LCN Dispersions for 6 h

Formulation code	CH_2 asymmetric stretching	CH_2 symmetric stretching	C=O stretching	CH_2 scissoring
Distilled water	2918.5±0.3	2850.7±0.2	1736.9±0.8	1457.0±0.3
RH 0.5	2924.9±0.7	2853.4±0.5	1745.0±0.3	1461.2±0.5
RH 2.5	2925.7±1.0	2853.6±0.3	1744.8±0.2	1459.0±4.8
EL 1.5	2925.8±0.8	2854.1±0.3	1743.2±2.1	1462.2±0.1
EL 4.0	2926.3±0.5	2854.0±0.1	1744.7±0.1	1461.9±0.2
P407	2925.4±0.7	2853.7±0.1	—	1454.7±0.6

Each value represents the mean±SD (n=6)

DISCUSSION

Surfactants are considered as the important constituents that affect the physical stability of LCN. To date, the most widely used surfactant for the stabilization of LCN is P407 which is composed of polyethylene oxide (PEO)-polypropylene oxide (PPO)-polyethylene oxide (PEO) block copolymer (26). The hydrophobic portion (PPO) is responsible for the anchoring to lipid bilayer, and hydrophilic portion (PEO) is oriented toward the aqueous medium. Stabilizing effect of P407 is attributed to the balance between the hydrophobic domain size of PPO and hydrophilic chain length of PEO (27). Surfactants with similar structural property would be expected to stabilize LCN efficiently as well. In this regard, we anticipated that the two polyoxyethylated nonionic surfactants (RH and EL) which have PEO moiety attached to hydrophobic region usually being fatty acids would also stabilize LCN dispersion. Hence, we aimed to investigate the effects of RH and EL on stabilization of LCN and topical delivery of FNS.

Herein, we have successfully prepared LCN dispersion stabilized by RH and EL using ultrasonication method. This result indicates that RH and EL are comparable to P407 in terms of stabilization of LCN dispersion. The stabilizing effect of RH and EL might be attributed to the balance between hydrophilic and hydrophobic moieties. Hydrophilic moiety of both RH and EL is composed of PEO which acts as a steric barrier to prevent aggregation of nanoparticles, and hydrophobic moiety is composed of stearate for RH and ricinoleate for EL, respectively, which have different affinity property to bind with lipid bilayer (26). Among the concentrations of RH and EL tested, RH formed stable dispersion as low as 0.5% *w/w* concentration while EL failed to stabilize the dispersion at lower than 1.5% *w/w* concentration (Table I). This difference in the stabilization efficiency might be due to number of PEO units, as RH has 40 units and EL contains

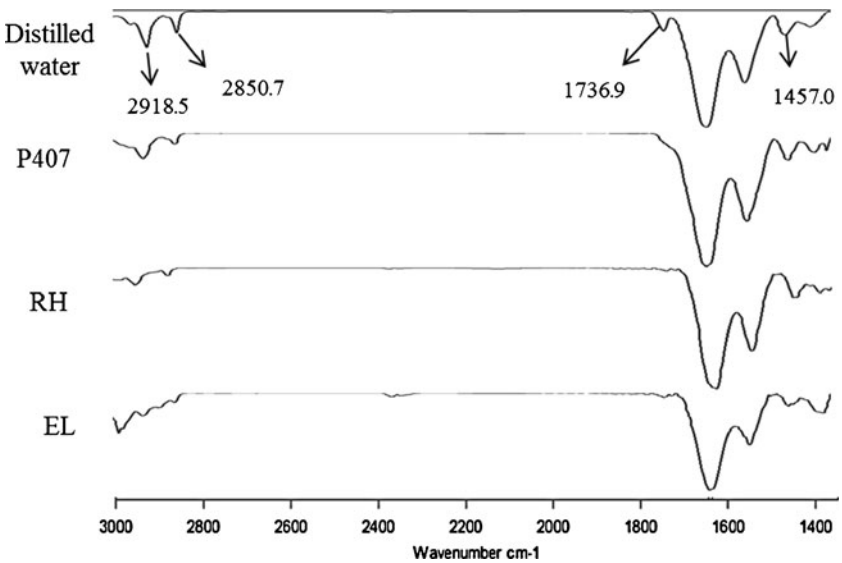

Fig. 5. FTIR spectra of porcine skin treated with distilled water and LCN formulations

35 units, respectively. It has been already reported that increase in the hydrophilic units of stabilizer appears to be sufficient to stabilize LCN even at low concentration (27).

In our earlier study, we reported that FNS-loaded LCN was successfully prepared by using MO and P407, and the concentration of additives affected drug release, skin permeation, and skin retention parameters of the drug. In this study, we prepared FNS-loaded LCN by using Cremophor in the place of P407 and found that the flux and enhancement ratio were in the range of 0.027–0.100 and 1.86–6.88 while those of the LCN prepared with MO and P407 were in the range of 0.018–0.067 and 1.04–3.70, respectively (21). Although direct comparison is not possible due to the difference in the concentrations of the additives and animal skin used, it appears that FNS-loaded LCNs prepared with Cremophor are not inferior to the LCNs prepared with P407.

TEM morphology of LCN prepared with different surfactants appears like spherical flower-like structure with multiple black dots, which represent phosphotungstic acid-staining of internal water channels (28). The appearance of these multiple black dots was believed to be formation of liquid crystalline phase. The observed nanoparticles in TEM showed slightly smaller in size compared with hydrodynamic size characterization. This was in accordance with the results obtained by previous researcher's finding that drying of the dispersion caused slight decrease in the particle size (29).

Among all parameters, surfactant concentration plays major role in influencing drug release from nanoparticles. The faster release by increasing surfactant concentration may be attributed to the more surfactant molecules available for the partitioning into the interfacial domain of liquid crystalline phase which results in swelling of internal curvature. Overall, all the formulation showed sustained release profile. This suggests that, in addition to the surfactant concentration, the hydrophobic interaction of FNS with the hydrophobic domain of LCN may play an important role in determining the release rate of drug from LCN. It has been already postulated by other authors that hydrophobic molecules show sustained release profile from LCN carrier (19).

Skin permeation studies showed a significant increase in the FNS permeation in the higher concentration of surfactants. Higher surfactant concentration causes increase in the fluidity of the membrane and eventually increase the permeation of drug. It has therefore been suggested that a dose-dependent increase in the permeability of SC is responsible for the surfactant-induced permeability of drug. However, significantly increased retention was observed at lower concentrations of the two surfactants (RH and EL). This finding is not fully understood at present, but it appears that too much increase in the skin cell membrane fluidity is not in favor of skin retention of FNS. So, further research is warranted to elucidate exact reason for the inconsistency in the permeation and retention of the drug in skin. The skin permeation and retention may also be affected by particle size, surface charge, and viscosity of formulations. However, there was no significant difference observed on particle size, zeta potential, and viscosity among the formulations.

Attenuated total reflectance Fourier-transform infrared spectroscopy (ATR-FTIR) spectroscopic studies were performed to study the formulation effect on the biophysical properties of the stratum corneum (30). It has been already demonstrated that porcine skin is very close to human skin in structural and chemical properties and a very helpful model for the transdermal drug diffusion study in combination with FTIR (31). Among the spectral bands of porcine skin, CH_2 bands (asymmetrical, symmetrical, and scissoring) are the absorbance of hydrocarbon chains of stratum corneum lipids and keratin (32). Study of these vibrational bands would provide insight information about the lipid order–disorder caused by different formulations. Our study demonstrates that all the formulations shifted the spectral bands to higher wavenumbers which result in a blue shift of CH stretching. This may be due to the increase in the degree of disorder of the lipid acyl chains, resulting in the increased fluidity of SC (33).

CONCLUSIONS

Thus far, FNS-loaded LCN was successfully prepared by sonication technique. In the present study, Cremophor concentration was optimized with regard to the stability of LCN. The surfactants were observed to have a significant influence on the drug release and skin permeability of FNS. To be specific, LCN prepared with RH exhibited markedly higher skin permeability than EL surfactant. It is noteworthy that the lower concentration of both the surfactants portrayed enhanced skin retention of FNS. These observations clearly suggest that the Cremophor surfactants can be utilized to stabilize the LCN for the topical delivery of FNS.

ACKNOWLEDGMENTS

This work was supported by the Gachon University research fund of 2012 (GCU-2012-M077).

REFERENCES

1. Tsuboi R, Itami S, Inui S, Ueki R, Katsuoka K, Kurata S, *et al.* Guidelines for the management of androgenetic alopecia (2010). J Dermatol. 2012;39(2):113–20.
2. Yamazaki M, Miyakura T, Uchiyama M, Hobo A, Irisawa R, Tsuboi R. Oral finasteride improved the quality of life of androgenetic alopecia patients. J Dermatol. 2011;38(8):773–7.
3. El-Domyati M, Attia S, Saleh F, Abdel-Wahab H. Androgenetic alopecia in males: a histopathological and ultrastructural study. J Cosmet Dermatol. 2009;8(2):83–91.
4. Inui S, Itami S. Androgen actions on the human hair follicle: perspectives. Exp Dermatol. 2012. doi:10.1111/exd.12024.
5. Azzouni F, Zeitouni N, Mohler J. Role of 5a-reductase inhibitors in androgen-stimulated skin disorders. J Drugs Dermatol. 2013;12(2):e30–5.
6. Gur S, Kadowitz PJ, Hellstrom WJ. Effects of 5-alpha reductase inhibitors on erectile function, sexual desire and ejaculation. Expert Opin Drug Saf. 2013;12(1):81–90.
7. Irwig MS. Persistent sexual side effects of finasteride: could they be permanent? J Sex Med. 2012;9(11):2927–32.
8. Tabbakhian M, Tavakoli N, Jaafari MR, Daneshamouz S. Enhancement of follicular delivery of finasteride by liposomes and niosomes 1. In vitro permeation and in vivo deposition studies using hamster flank and ear models. Int J Pharm. 2006;323(1–2):1–10.
9. Javadzadeh Y, Shokri J, Hallaj-Nezhadi S, Hamishehkar H, Nokhodchi A. Enhancement of percutaneous absorption of finasteride by cosolvents, cosurfactant and surfactants. Pharm Dev Technol. 2010;15(6):619–25.
10. Alexander A, Dwivedi S, Ajazuddin, Giri TK, Saraf S, Tripathi DK. Approaches for breaking the barriers of drug permeation through transdermal drug delivery. J Control Release. 2012;164(1):26–40.

11. Prow TW, Grice JE, Lin LL, Faye R, Butler M, Becker W, *et al*. Nanoparticles and microparticles for skin drug delivery. Adv Drug Deliv Rev. 2011;63(6):470–91.
12. Schafer-Korting M, Mehnert W, Korting HC. Lipid nanoparticles for improved topical application of drugs for skin diseases. Adv Drug Deliv Rev. 2007;59(6):427–43.
13. Gan L, Han S, Shen J, Zhu J, Zhu C, Zhang X, *et al*. Self-assembled liquid crystalline nanoparticles as a novel ophthalmic delivery system for dexamethasone: improving preocular retention and ocular bioavailability. Int J Pharm. 2010;396(1–2):179–87.
14. Lopes LB, Ferreira DA, de Paula D, Garcia MT, Thomazini JA, Fantini MC, *et al*. Reverse hexagonal phase nanodispersion of monoolein and oleic acid for topical delivery of peptides: in vitro and in vivo skin penetration of cyclosporin A. Pharm Res. 2006;23(6):1332–42.
15. Bender J, Simonsson C, Smedh M, Engstrom S, Ericson MB. Lipid cubic phases in topical drug delivery: visualization of skin distribution using two-photon microscopy. J Control Release. 2008;129(3):163–9.
16. Rizwan SB, Dong YD, Boyd BJ, Rades T, Hook S. Characterisation of bicontinuous cubic liquid crystalline systems of phytantriol and water using cryo field emission scanning electron microscopy (cryo FESEM). Micron. 2007;38(5):478–85.
17. Rizwan SB, McBurney WT, Young K, Hanley T, Boyd BJ, Rades T, *et al*. Cubosomes containing the adjuvants imiquimod and monophosphoryl lipid A stimulate robust cellular and humoral immune responses. J Control Release. 2013;165(1):16–21.
18. Yaghmur A, Glatter O. Characterization and potential applications of nanostructured aqueous dispersions. Adv Colloid Interface Sci. 2009;147–148:333–42.
19. Nguyen TH, Hanley T, Porter CJ, Boyd BJ. Nanostructured liquid crystalline particles provide long duration sustained-release effect for a poorly water soluble drug after oral administration. J Control Release. 2011;153(2):180–6.
20. Boyd BJ, Dong YD, Rades T. Nonlamellar liquid crystalline nanostructured particles: advances in materials and structure determination. J Liposome Res. 2009;19(1):12–28.
21. Madheswaran T, Baskaran R, Thapa RK, Rhyu JY, Choi HY, Kim JO, *et al*. Design and in vitro evaluation of finasteride-loaded liquid crystalline nanoparticles for topical delivery. AAPS PharmSciTech. 2013;14(1):45–52.
22. Hashem FM, Shaker DS, Ghorab MK, Nasr M, Ismail A. Formulation, characterization, and clinical evaluation of microemulsion containing clotrimazole for topical delivery. AAPS PharmSciTech. 2011;12(3):879–86.
23. Thomas N, Holm R, Mullertz A, Rades T. In vitro and in vivo performance of novel supersaturated self-nanoemulsifying drug delivery systems (super-SNEDDS). J Control Release. 2012;160(1):25–32.
24. Chen YC, Liu DZ, Liu JJ, Chang TW, Ho HO, Sheu MT. Development of terbinafine solid lipid nanoparticles as a topical delivery system. Int J Nanomedicine. 2012;7:4409–18.
25. Moghadam SH, Saliaj E, Wettig SD, Dong C, Ivanova MV, Huzil JT, *et al*. Effect of chemical permeation enhancers on stratum corneum barrier lipid organizational structure and interferon alpha permeability. Mol Pharm. 2013;10(6):2248–60.
26. Chong JY, Mulet X, Waddington LJ, Boyd BJ, Drummond CJ. Steric stabilisation of self-assembled cubic lyotropic liquid crystalline nanoparticles: high-throughput evaluation of triblock polyethylene oxide-polypropylene oxide-polyethylene oxide copolymers. Soft Matter. 2011;7:4768–77.
27. Chong JY, Mulet X, Waddington LJ, Boyd BJ, Drummond CJ. High-throughput discovery of novel steric stabilizers for cubic lyotropic liquid crystal nanoparticle dispersions. Langmuir. 2012;28(25):9223–32.
28. Zeng N, Hu Q, Liu Z, Gao X, Hu R, Song Q, *et al*. Preparation and characterization of paclitaxel-loaded DSPE-PEG-liquid crystalline nanoparticles (LCNPs) for improved bioavailability. Int J Pharm. 2012;424(1–2):58–66.
29. Gaumet M, Vargas A, Gurny R, Delie F. Nanoparticles for drug delivery: the need for precision in reporting particle size parameters. Eur J Pharm Biopharm. 2008;69(1):1–9.
30. Hasanovic A, Winkler R, Resch GP, Valenta C. Modification of the conformational skin structure by treatment with liposomal formulations and its correlation to the penetration depth of aciclovir. Eur J Pharm Biopharm. 2011;79(1):76–81.
31. Kong R, Bhargava R. Characterization of porcine skin as a model for human skin studies using infrared spectroscopic imaging. Analyst. 2011;136(11):2359–66.
32. Schwarz JC, Pagitsch E, Valenta C. Comparison of ATR-FTIR spectra of porcine vaginal and buccal mucosa with ear skin and penetration analysis of drug and vehicle components into pig ear. Eur J Pharm Sci. 2012. doi:10.1016/j.ejps.2012.12.020.
33. Bhatia KS, Gao S, Freeman TP, Singh J. Effect of penetration enhancers and iontophoresis on the ultrastructure and cholecystokinin-8 permeability through porcine skin. J Pharm Sci. 1997;86(9):1011–5.